CALCULATION OF MECHANICAL AND THERMAL INFLUENCES DURING COILING OF HOT STRIP

V. SATTINGER[*], A. KAINZ[†], K. SCHÖRKHUBER[♦], L. AIGNER[♦] AND K. ZEMAN[†]

[*] Institute of Mechatronic Design and Production
Johannes Kepler University Linz
Altenbergerstraße 69, A-4040 Linz, Austria
E-mail: vinzenz.sattinger@jku.at, Web page: http://came.mechatronik.uni-linz.ac.at

[♦] voestalpine Stahl GmbH, voestalpine-Str. 3, A-4020 Linz, Austria
E-mail: karl.schoerkhuber@voestalpine.com, Web page: http://www.voestalpine.com/stahl/en

[†] Institute of Mechatronic Design and Production
Johannes Kepler University Linz
Altenbergerstraße 69, A-4040 Linz, Austria
E-mail: klaus.zeman@jku.at, Web page: http://came.mechatronik.uni-linz.ac.at

Key words: Coiling of Hot Strip, Strip Flatness, Residual Stresses, Hyperelasto-plastic Deformation, Solid Shell Elements, Locking phenomena.

Abstract. Coiled steel strip is the final product from flat hot rolling processes. With increasing demand for higher quality of hot rolled strips, especially the evolution of strip flatness during and after coiling becomes a crucial aspect. The main impacts on the flatness properties of hot rolled strips result from residual stresses and "eigen-strains" induced by the last hot rolling passes, by strip cooling at the run-out table, and finally, by the mechanical and thermal conditions during and after the coiling process itself. In this paper, a mathematical model is presented, which takes into account the mechanical and thermal effects on hot rolled strip during and after the coiling process. To improve the prediction quality of the underlying process, a customized self-developed 3D finite-element model has been developed and programmed in C++, leading to a software prototype, which is highly superior to commercial FEM-packages with respect to calculation time and storage capacities. The model is based on a dynamic implicit total Lagrangian formulation. All relevant devices directly interacting with the strip, such as pinch rolls, coiler rolls and mandrel are incorporated in the calculation model. Well known and established methods in the solid-shell theory, like the EAS- and ANS-method, were applied to prevent the occurrence of locking phenomena resulting from low order interpolation functions. Selected benchmark tests were performed to evaluate the accuracy of these novel solid-shell elements in comparison to the results attained by the FEM-package ABAQUS[©]. The results obtained so far agree very satisfactorily. A further important topic is the contact and friction algorithm, where Coulomb's friction law is applied. The accurate and reliable determination of the contact between strip and interacting devices as well as the aspect of self-contact was treated by applying a sophisticated two dimensional contact search algorithm, leading to a significantly reduced calculation time. The highly non-linear time-dependent system of equations is integrated by utilizing the (implicit) Newmark

time-integration scheme. The developed calculation model serves as an effective tool to predict the interesting stress-distributions and local plastic deformations inside the strip, which induce residual stresses and strip unflatness (latent or even manifest waviness). Furthermore, this tool provides the basis for further improvements and investigations on hot rolling production lines.

1 INTRODUCTION

To fulfill the requirements of customers of hot rolled strip, the improvement of the product quality is always one of the main objectives pursued by steel strip manufacturers. Therefore, many researchers in the field of steel strip manufacturing try to understand and predict the highly non-linear thermo-mechanical effects causing strip flatness defects.

One of the first investigations was performed in an empiric way by Blazevic [3, 4] in the 1980's. In his work he describes the setup of all devices interacting with the strip during the coiling process. Elaborate investigations were also made for coiling of cold rolled steel strip for example in [6, 9, 10, 11, 15], whereas the influence of temperature is widely not taken into account, hence, being of less relevance for coiling of hot strip. The focus of these papers lies on residual stresses (spring-back analysis) of the unwound strip and on the pressure distribution during the coiling process of magnetic, cold rolled steel sheets. Other researchers focus on down-cooling processes on the cooling-stage [7, 14, 18]. Due to the high temperature well above 600°C on the cooling line input side, the influence of phase transitions is also a crucial aspect in their investigations including metallurgical aspects. These models take into account the coupled thermo-metallurgical effects. Most of them are implemented in a finite-element calculation model. The results show that the influence of arising residual stresses in strip-width direction is much smaller than in strip-length direction, whereas tensile stresses at the strip-edges are caused by residual stresses in strip-length direction in contrast to compressive stresses near the strip center.

After an extensive literature study and careful evaluations of a lot of scientific publications, no appropriate studies were found, which investigated the coupled mechanical and thermal effects during the coiling of hot strip. Nevertheless, a preliminary assessment can be done to estimate the relevant quantities during the coiling procedure for the following modelling and simulation. External mechanic and thermal influences on the strip are essential and need to be taken into account, whereas phase transitions can be neglected for a coiling temperature below about 600°C. Extreme temperature differences on the cooling-stage between the strip center and the edges have a significantly negative effect on strip flatness. This also holds true during and after the coiling process. Note that uneven length stress distributions in strip-width directions also have tremendous effects on strip flatness.

1.1 Objectives

The aim of this study is to develop a finite-element calculation program to investigate the influence of back tension, coiling speed, strip material, coiler geometry, cooling rate etc. on coil quality and strip flatness. Subsequently, this permits an optimization of the coiler input parameters like temperature, tension profile over the strip width, strip geometry etc. and finally leads to an improved coil and strip quality. Furthermore, the model should be able to predict the required amount of force and power.

2 ESSENTIAL MODELING ASPECTS

A brief overview of the coiling process is shown in Figure 1. During the thread-in process, the strip-head with a temperature of approximately 600°C is fed to the mandrel by the lower and upper pinch roll. The adjustable coiler rolls, assisted by the coiler guides, push the strip against the mandrel and thus ensure sufficient frictional forces to wrap the strip around the mandrel. Two things have to be considered for a continuous coiling process. At first, a homogeneous and continual strip tension has to be applied by the mandrel to ensure that there is enough tension between the last rolling stand and the mandrel itself. Secondly, tight quality requirements imply close tolerances for winding up a coil. Before the end of the strip is reached, it is decelerated and the strip-tail will be brought into the right position by the mandrel (see the right picture in Figure 1). The coil conveyor moves up and pulls the coil off the mandrel. The coil represents either the finished product, or it will be passed on to further process steps (e.g. cold rolling).

Regarding the numerical simulation of the coiling and uncoiling process, a certain number of conclusions can be drawn:

- Strains in strip thickness direction have to be taken into account, due to the expected high pressure in radial direction.
- As a result of the geometry, large local deformations in combination with large rotations have to be considered.
- Significant temperature dependency of the material parameters, especially concerning the yield strength $k_f(T)$, leads to a coupled thermo-mechanical system.
- Heat generation caused by plastic deformation during coiling itself and also due to friction between the coiler devices and the strip can be neglected.
- Due to the expected high number of degrees of freedom of the coupled problem, low order interpolation functions (preferably linear or quadratic) should be used.
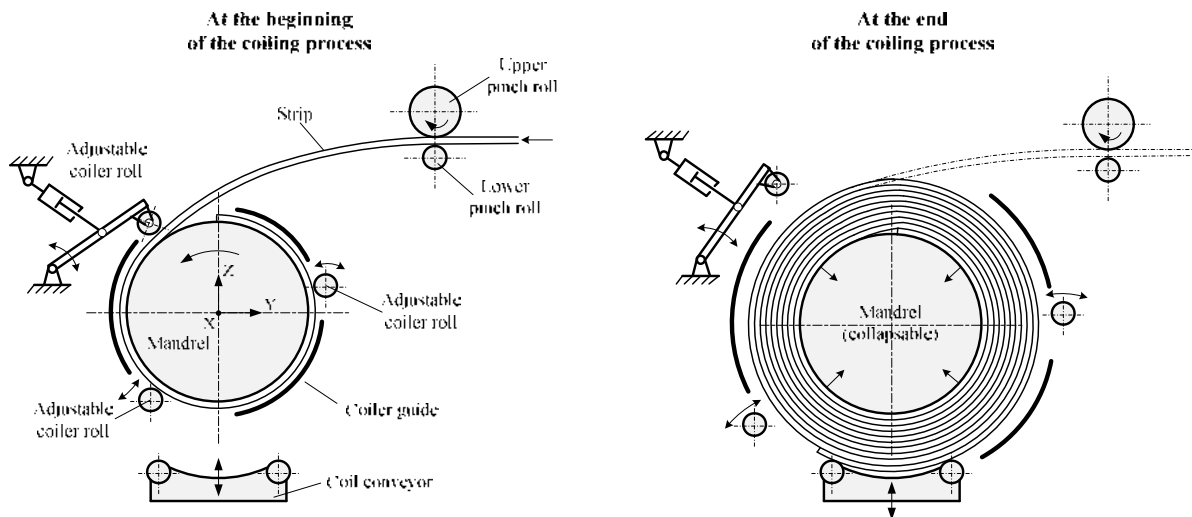

Figure 1: Coiling process

Based on these assumptions, solid-shell elements will be used for strip discretization,

because these elements take into account the full three dimensional stress-state (in contrast to classical shell elements) as they are well suited for this kind of problem. Many approaches are possible to construct solid-shell elements in accordance with the underlying mathematics, e.g. [5, 8, 13]. The basis of the solid-shell element development in this work is similar to the mathematics in Bischoff [2]. In extension to this work, which is restricted to small strains, a hyperelasto-plastic material law defined in principal strains will be used. The occurrence of locking phenomena resulting from low order interpolation functions will be prevented by the ANS (Assumed-Natural-Strains) and EAS (Enhanced-Assumed-Strains) method.

2.1 Solid shell element

An eight-node solid shell element (denoted by SS8) based on linear shape functions to interpolate the geometry and displacements is shown in Figure 2. The use of linear shape functions fulfills the Reissner-Mindlin kinematics. Alternatively, sixteen-node solid shell elements based on quadratic shape functions were also developed and implemented. Systematic numerical studies showed that the results attained by utilizing such even more sophisticated elements lead to an improved convergence behaviour and to a reduction of computational costs. Starting point for the discretization is the variational form of the Hu-Washizu two field functional in the Total-Lagrangian form

$$\delta\Pi_{HW} = \int_{\Omega_0} \frac{\partial W(\mathbf{E}^u + \widetilde{\mathbf{E}})}{\partial(\mathbf{E}^u + \widetilde{\mathbf{E}})} : \delta(\mathbf{E}^u + \widetilde{\mathbf{E}}) dV + \delta\Pi^{ext} = 0, \qquad (1)$$

which includes the compatible part of the Green-Lagrangian strains $\mathbf{E}^u$ (derivation with respect to the displacements) and the incompatible part of the Green-Lagrangian strains $\widetilde{\mathbf{E}}$ (see also [13, 16]). W denotes an appropriate hyperelasto-plastic strain energy functional (cf. e.g. [2, 16]). An arbitrary point at the initial (Lagrangian $\mathbf{R}$) and current (Eulerian $\mathbf{r}$) configuration within the shell continuum is expressed by the position vectors

$$\mathbf{R} = \mathbf{R}_m + \theta_3 \mathbf{A}_3 \qquad (2)$$

$$\mathbf{r} = \mathbf{r}_m + \theta_3 \mathbf{a}_3,$$

where $\mathbf{R}_m$, $\mathbf{r}_m$ describe the position of the shell's mid plane (subscript m) and, $\mathbf{A}_3$ and $\mathbf{a}_3$ the basis vectors in thickness direction. Furthermore, all basis vectors and corresponding coordinates within the shell continuum are given by (cf. Figure 2):
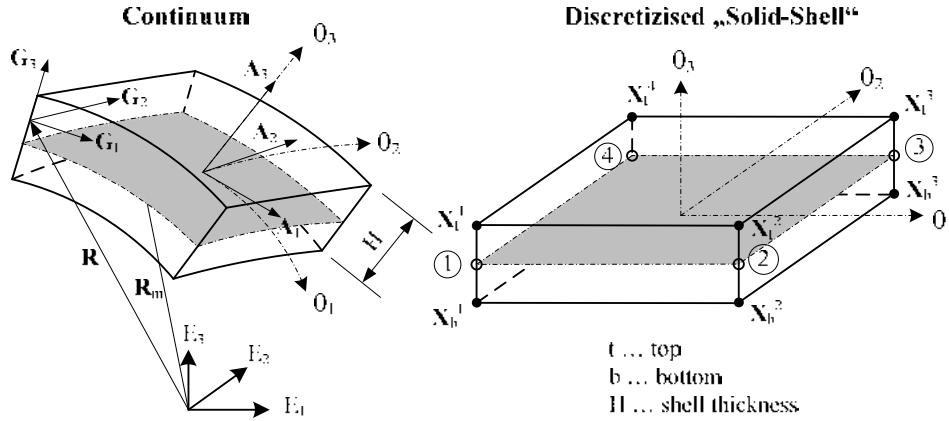
$$\mathbf{G}_1 = \mathbf{A}_1 + \theta_3 \mathbf{A}_{3,1} \qquad \mathbf{g}_1 = \mathbf{a}_1 + \theta_3 \mathbf{a}_{3,1} \qquad (3)$$

$$\mathbf{G}_2 = \mathbf{A}_2 + \theta_3 \mathbf{A}_{3,2} \qquad \mathbf{g}_2 = \mathbf{a}_2 + \theta_3 \mathbf{a}_{3,2}$$

$$\mathbf{G}_3 = \mathbf{A}_3 \qquad \mathbf{g}_3 = \mathbf{a}_3,$$

with $\mathbf{A}_{3,k}$ being the derivative of $\mathbf{A}_3$ with respect to θ_k. By the use of linear shape functions

$$N_K = 0,25(1 + \theta_1^K \theta_1)(1 + \theta_2^K \theta_2) \qquad K = 1...4, \qquad (4)$$

the discrete form of the basis vectors acting on the middle plane can be written as:

$$\mathbf{A}_i = 0,5\,N_{K,i}\left(\mathbf{X}_t^K + \mathbf{X}_b^K\right) \qquad \mathbf{a}_i = \mathbf{A}_i + 0,5\,N_{K,i}\left(\mathbf{u}_t^K + \mathbf{u}_b^K\right)$$

$$\mathbf{A}_{3,i} = 0,5\,N_{K,i}\left(\mathbf{X}_t^K - \mathbf{X}_b^K\right) \qquad \mathbf{a}_{3,i} = \mathbf{A}_{3,i} + 0,5\,N_{K,i}\left(\mathbf{u}_t^K - \mathbf{u}_b^K\right), \tag{5}$$

Figure 2: Kinematics and discretization of an 8-node solid shell element

where $\mathbf{X}_{t,b}^i$ denotes the coordinates and $\mathbf{u}_{t,b}^i$ the displacements of the nodes. Now the displacement based covariant components of the Green-Lagrangian strain tensor $\overline{\mathbf{E}}_{ij}^u = 0,5\left(\mathbf{g}_i \cdot \mathbf{g}_j - \mathbf{G}_i \cdot \mathbf{G}_j\right)$ can be determined. These covariant components will be expanded by the incompatible part $\widetilde{E}_{ij}$ in an additive way (EAS method), whereas the covariant components of the total strains can be calculated from:

$$\overline{E}_{ij} = \overline{E}_{ij}^u + \widetilde{E}_{ij} = \alpha_{ij}^u + 0,5H\,\theta_3\,\beta_{ij}^u + 0,25H^2\,\theta_3^2\,\gamma_{ij}^u + \widetilde{E}_{ij}. \tag{6}$$

They include the kinematic variables α_{ij}^u, β_{ij}^u and γ_{ij}^u (cf. [2]) resulting from the decomposition with respect to the thickness coordinate θ_3. All these kinematic variables are acting on the middle plane and can be interpreted as normal, membrane and shear strains. Additionally, also strains of higher order appear, which is in contrast to the linear shell theory. The crucial step for calculation of the nonlinear internal forces is the decomposition of the volume integral into an integral over the middle plane and the shell thickness according to:

$$\int_{\Omega_0}(\bullet)\,dV = \int_{\partial\Omega_0}\int_{-1}^{1}(\bullet)\,\hat{\mu}\,d\theta_3\,dA \qquad \hat{\mu} = \frac{(\mathbf{g}_1 \times \mathbf{g}_2)\cdot\mathbf{g}_3}{\|\mathbf{a}_1 \times \mathbf{a}_2\|}. \tag{7}$$

The static variables n^{ij}, m^{ij} und s^{ij} which are conjugate in energy to the kinematic variables are calculated from the contra variant components $\overline{S}^{ij}$ of the 2nd Piola-Kirchhoff stresses:

$$n^{ij} = \int_{-1}^{1}\overline{S}^{ij}\hat{\mu}\,d\theta_3, \qquad m^{ij} = \int_{-1}^{1}0,5H\,\theta_3\,\overline{S}^{ij}\hat{\mu}\,d\theta_3, \qquad s^{ij} = \int_{-1}^{1}0,25H^2\,\theta_3^2\,\overline{S}^{ij}\hat{\mu}\,d\theta_3. \tag{8}$$

Consequently, Equation 1 can be rearranged in vector notation

$$\delta\Pi_{HW} = \int_{\partial\Omega_0}\left[\mathbf{S}_s \cdot \delta\mathbf{E}_k^u + \mathbf{S}_s \cdot \delta\widetilde{\mathbf{E}}_k\right]dA + \delta\Pi^{ext} = 0,$$

(9)

with the vectors of kinematic and static variables:

$$\mathbf{S}_S = \begin{bmatrix} n^{11} & n^{22} & \cdots & s^{12} \end{bmatrix}^T \qquad \mathbf{E}_k^u = \begin{bmatrix} \alpha_{11}^u & \alpha_{22}^u & \cdots & 2\gamma_{12}^u \end{bmatrix}^T.$$

(10)

2.2 Avoidance of locking phenomena

The EAS method will be used to prevent volumetric locking. The imbalance of the normal strains $\overline{E}_{11}^u$, $\overline{E}_{22}^u$ and $\overline{E}_{33}^u$ is remedied by the incompatible strains $\widetilde{E}_{ii}$. Hence, the vector of the kinematic variables in vector notation is supplemented by the additional three degrees of freedom α_1, α_2 and α_3:

$$\delta\widetilde{\mathbf{E}}_k = \begin{bmatrix} \widetilde{\alpha}_{11} \\ \widetilde{\alpha}_{22} \\ \vdots \\ \widetilde{\beta}_{33} \\ \vdots \end{bmatrix} = \begin{bmatrix} 0 & \theta_1 & 0 \\ 0 & 0 & \theta_2 \\ \vdots & \vdots & \vdots \\ 1 & 0 & 0 \\ \vdots & \vdots & \vdots \end{bmatrix}\begin{bmatrix} \alpha_1 \\ \alpha_2 \\ \alpha_3 \end{bmatrix} = \mathbf{M}\,\boldsymbol{\alpha}$$

(11)

The ANS method will be used to prevent the shear and thickness locking phenomenoa which have a negative effect on the element response especially in bending applications. For this purpose, special evaluation points on A, B, C and D for calculating the shear strains α_{23}^u and α_{13}^u and E, F, G, H for calculating the thickness strains α_{33}^u are selected and subsequently interpolated over the continuum (see Figure 3).
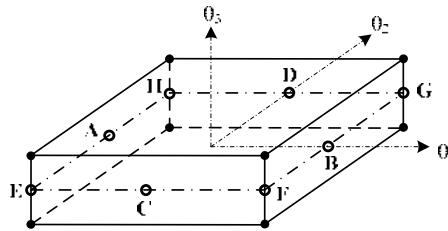
Figure 3: Evaluation points of the ANS method

This leads to the new shear and thickness strains:

$$\alpha_{23}^{u,ANS} = 0{,}5\left(1-\theta_1\right)\alpha_{23}^{u,A} + 0{,}5\left(1+\theta_1\right)\alpha_{23}^{u,B}$$

(12)

$$\alpha_{13}^{u,ANS} = 0{,}5\left(1-\theta_2\right)\alpha_{13}^{u,C} + 0{,}5\left(1+\theta_2\right)\alpha_{13}^{u,D}$$

(13)

$$\alpha_{33}^{u,ANS} = N_E \, \alpha_{33}^{u,E} + N_F \, \alpha_{33}^{u,F} + N_G \, \alpha_{33}^{u,G} + N_H \, \alpha_{33}^{u,H} \tag{14}$$

$$\text{with } N_K = 0{,}25 \left(1 + \theta_1^K \theta_1\right)\left(1 + \theta_2^K \theta_2\right) \qquad K = E, F, G, H.$$

The shear and thickness strains $\alpha_{23}^{u,ANS}, \alpha_{13}^{u,ANS}$ and $\alpha_{33}^{u,ANS}$ obtained in this way, substitute the strains α_{23}^{u}, α_{13}^{u} and α_{33}^{u} in Equation 6.

2.3 Hyperelasto-plastic material law

The contra variant components $\bar{S}^{ij}$ in Equation 8 are calculated from the constitutive relation and depend in the case of hyperelastic material on the strain energy functional

$$W = W(\lambda_1, \lambda_2, \lambda_3), \tag{15}$$

which is defined in principal strains λ_i (see also [1, 2, 16]). Based on the spectral decomposition of the 2. Piola-Kirchhoff stress tensor

$$\mathbf{S} = \sum_{i=1}^{3} S_i \, \mathbf{N}_i \otimes \mathbf{N}_i, \tag{16}$$

the contra variant components $\bar{S}^{ij}$ can be calculated after some transformations. In the case of hyperelasto-plastic material, the new stresses at time step $t = n+1$ will be calculated by using a predictor-corrector algorithm. After applying some rearrangement on Equation 6 and taking into account the Levy-Mises flow rule, the elastic predictor can be written as:

$$\mathbf{C}_{n+1}^{e,Trial} = \mathbf{C}_n^{p-1} \, \mathbf{C}_{n+1}. \tag{17}$$

The crucial step is that the right Cauchy-Green strains $\mathbf{C}_{n+1}$ has to be calculated from Equation 6, which includes all relevant modifications caused by the ANS method. Afterwards, the principal strains $\lambda_i^{e,Trial}$ will be calculated from the elastic trial strains $\mathbf{C}_{n+1}^{e,Trial}$ resulting from Equation 17 and subsequently substituted in the strain energy function (Equation 15) for evaluation of the stresses $\bar{S}^{ij}$. Concerning the thermo-mechanical coupling the following approach

$$J^e = J \exp\left[-3\alpha_L (T - T_0)\right] \qquad J = \lambda_1 \lambda_2 \lambda_3 \tag{18}$$

as proposed by [12, 17] is used, which implies that heat has only a direct influence on the volumetric part of $\mathbf{C}$.

2.4 Contact

Within the contact zone a distinction is made between normal and tangential contact [17]. The impenetrability condition is applied in normal direction, whereas in tangential direction the Coulomb friction law is applied. Due to the expected high order system of equations it seems advantageous to use the penalty formulation for adding all contact contributions. The discretization of the contact surface between the mandrel and the strip is applied by using

node to surface contact elements (NTS-elements). The exact contact point is determined by the projection of the slave node (strip) onto the master surface (mandrel) as shown in Figure 4.
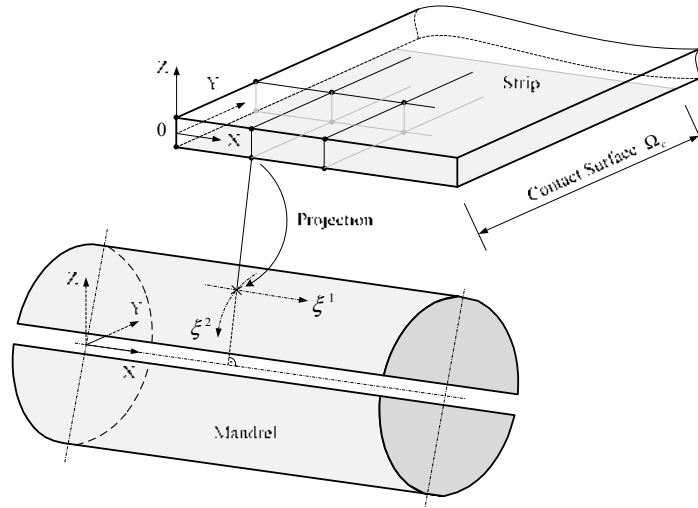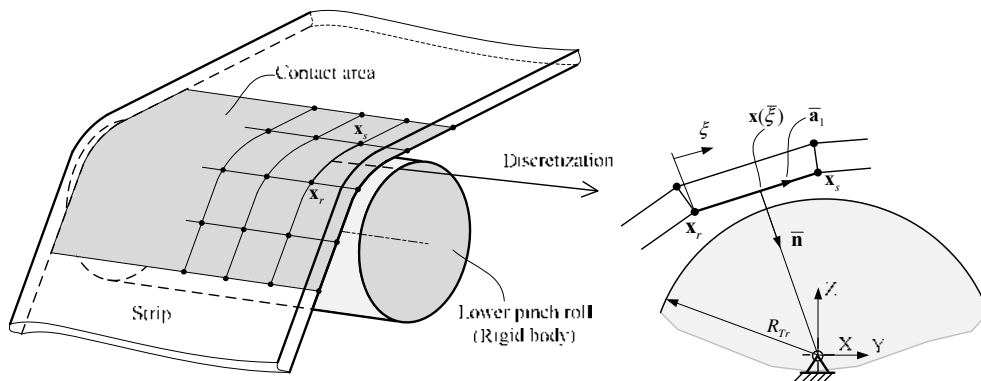

Figure 4: Contact between mandrel and strip

The mandrel is modelled as an isothermal slotted-cylinder representing a good approximation for the real device, which consists of four collapsible segments. The mechanical and thermal contact contributions of the contact surface Ω_c are supplied from the weak form

$$\delta\Pi_c + \delta\Pi_c^{Th} = \int_{\partial\Omega_c} \left(p_N \, \delta g_N + \mathbf{t}_T \cdot \delta\mathbf{g}_T \right) da + \int_{\partial\Omega_c} \varepsilon_T \, g_T \, \delta g_T \, da,$$

(19)

where p_N is the pressure, g_N the gap function, $\mathbf{t}_T$ the tangential shear stresses, $\mathbf{g}_T$ the tangential distance function, g_T the thermal gap function and ε_T the thermal penalty parameter.

Figure 5: Contact between pinch roll/coiler roll and strip

The pinch and coiler rolls are modelled as isothermal cylinders (Figure 5), whereas the contact zone is discretized by self-developed line to surface contact elements (LTS-elements). The friction in the contact zone is also modelled within the frame of Coulombs law. The idea behind the self-contact formulation due to wrapping is shown in Figure 6. An essential speed-up is gained by establishing an efficient global search algorithm. The master element wrapping around corresponding slave nodes is surrounded by a bounding sphere. If a slave node is positioned within the bounding sphere then a local algorithm determines the exact contact coordinates. The discretization concept is based on node to surface contact elements (NTS-elements).
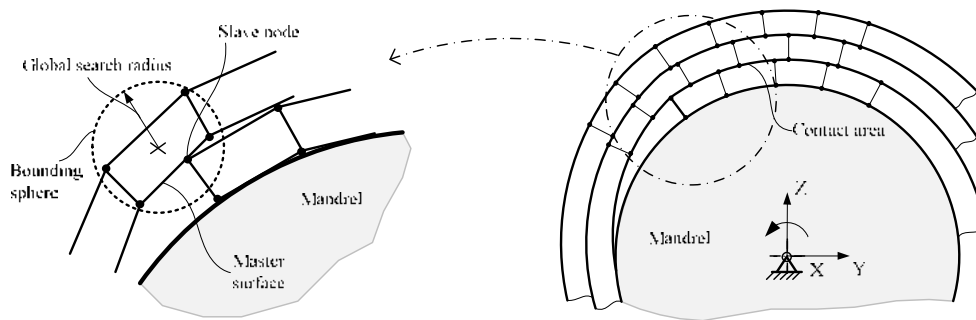

Figure 6: Determination of the contact pairs during self-contact

2.5 Global non-linear transient system of equations

A systematic expansion of Equation 9 including inertia and gravitation forces and performing a condensation of the EAS parameters on element level leads to the general form of the system of equations of motion

$$\mathbf{M}\,\ddot{\mathbf{u}}(t) + \mathbf{D}\,\dot{\mathbf{u}}(t) + \mathbf{R}(\mathbf{u}(t)) = \mathbf{P}(t), \tag{20}$$

where $\mathbf{M}$ is the mass matrix, $\mathbf{D}$ the damping matrix, $\mathbf{R}(\mathbf{u}(t))$ the vector of inner forces and $\mathbf{P}(t)$ the vector of external forces. The calculation of the temperature field, resulting from the heat balance equation leads to the equation system

$$\mathbf{M}_T\,\dot{\mathbf{T}}(t) + \mathbf{K}_T\,\mathbf{T}(t) + \mathbf{R}_T(\mathbf{T}(t)) = \mathbf{0}, \tag{21}$$

where $\mathbf{M}_T$ is the capacity matrix, $\mathbf{K}_T$ the conductivity matrix and $\mathbf{R}_T(\mathbf{T}(t))$ the heat flux vector. Both equation systems are solved implicitly in time. Note that for solving Equation 20 the Newmark method and for Equation 21 the implicit Euler method is used. All these algorithms are implemented in C++ in an object-oriented way, where finally the calculation program Coil-3D-MT is originated.

3 NUMERICAL APPLICATIONS

3.1 Element tests

Figure 7 shows a clamped beam for which the element response was tested in the static implicit case for elastic and elasto-plastic material.
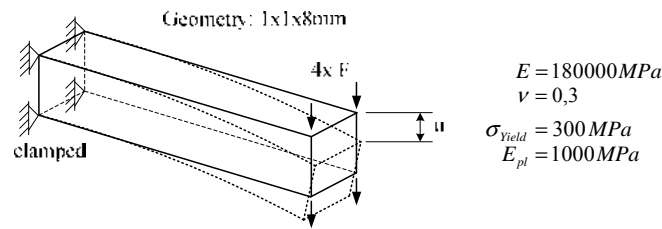
Figure 7: Deflection of a clamped beam

Table 1: Solid shell element test carried out on a cantilever

|	ABAQUS (C3D8R)			Coil-3D-M (SS8)		
	Mesh (Elements)	F [N]	u [mm]	Mesh (Elements)	F [N]	u [mm]
Elastic	5x5x40	40	1,77	1x1x1	40	1,36
				1x1x3	40	1,67
				1x1x10	40	1,76
Elasto-plastic	5x5x40	3,5	2,74	1x1x1	3,5	0,14
				1x1x3	3,5	1,93
				1x1x10	3,5	2,52

For this purpose, a fine mesh with 5x5x40 continuum elements (C3D8R) was generated in the commercial software package ABAQUS$^©$ and applied to the beam. The vertical tip deflection u after applying the external forces (Figure 7) is very close to the ABAQUS$^©$ solution confirming the correct response of the solid shell element SS8. Table 1 shows the convergence of the SS8 element with increasingly finer mesh in comparison to the ABAQUS$^©$ solution. The results demonstrate a very good approximation even for low element numbers involved. Beyond this, a lot of tests have been performed to evaluate the element behaviour under different load conditions. All of them turned out to be in satisfactory agreement with the ABAQUS$^©$ solution.

3.2 Coiling and uncoiling

Figure 8 shows the simulation results of the coiling and uncoiling process based on a dynamic-implicit and thermo-mechanical scheme. The strip velocity is constant throughout the coiling process, whereas an additional strip tension is applied between the pinch rolls and the mandrel, which is generated by external torques acting on the lower pinch roll and the mandrel. The boundary conditions on the strip-tail are imposed such that the strip is loaded by a back-tension unsymmetrical across the strip-width. After the coiling process, the mandrel decelerates, is stopped and holds its position until the temperature of the coil is lower than 200°C. Afterwards, the uncoiling process starts. Figure 9 shows the surface profile of the uncoiled strip. Obviously, the waves in lateral direction are induced due to the radial offset caused by the strip-head.
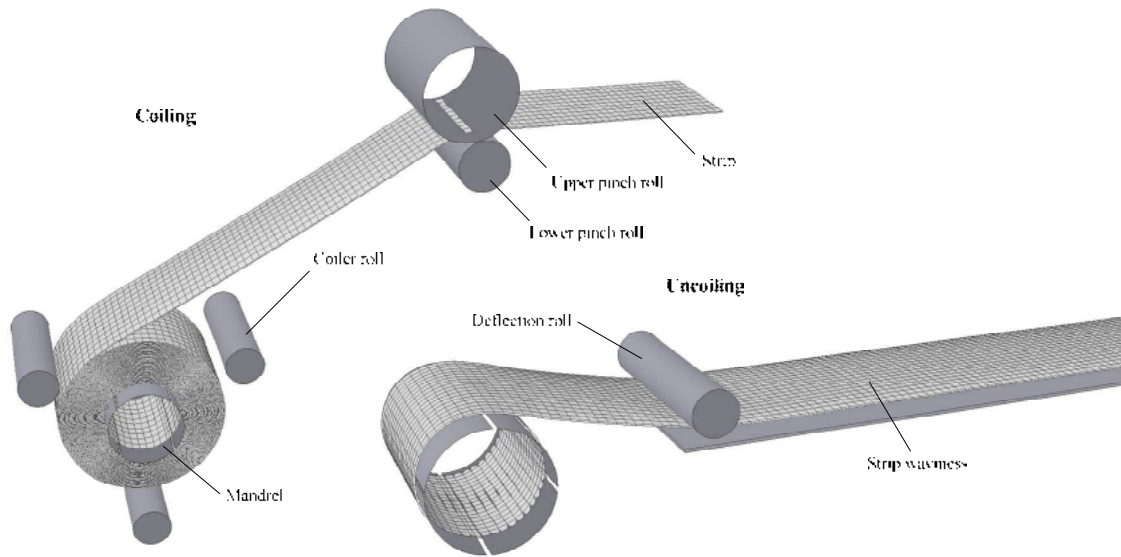
Figure 8: Coiling and uncoiling process
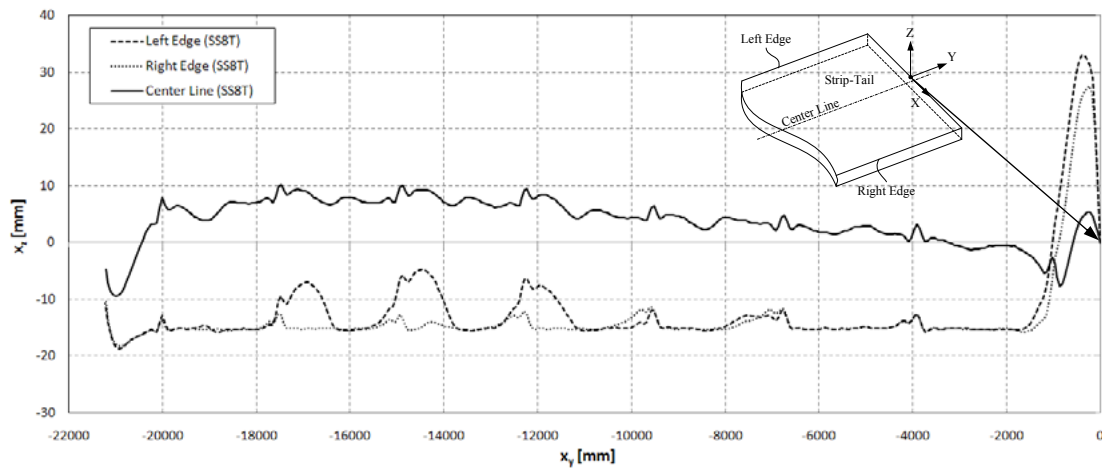
Figure 9: Strip flatness defects after uncoiling

4   CONCLUSIONS

The element formulation based on the solid shell concept turns out to be very efficient to calculate the coiling and uncoiling process. Several systematic element tests beyond the tests mentioned above, confirm the robustness and convergence in the static and dynamic case. The developed calculation tool *"Coil-3D-MT"* provides essential aspects to reduce strip waviness resulting from residual stresses. Further parameter studies need to be addressed to confirm the calculated results.

5   ACKNOWLEDGEMENT

voestalpine Stahl GmbH within the frame of this research project.

REFERENCES

[1] Bathe K.J.: *Finite Element Procedures*, Prentice Hall, New Jersey, (1996).

[2] Bischoff M.: *Theorie und Numerik einer dreidimensionalen Schalenelement-formulierung*, Institut for Structural Mechanics, University of Stuttgart, Technical report, (1999).

[3] Blazevic D.: *Hot Strip Mill Operations, Volume I*, Unpublished References, (1990).

[4] Blazevic D.: *Hot Strip Mill Coiling*, Unpublished References, (1982-1990).

[5] Choi K., Im S.: Finite element simulation of welding processes using a solid-shell element, *Journal of Physics* (2009) **42**:1-17.

[6] Domanti S., Edwards W.J., Voss G.F.: *Optimising coil winding*, Steel Times, (2000).

[7] Heung Nam Han, Jae Kon Lee, Hong Joon Kim, Young-Sool Jin: A model for deformation, temperature and phase transformation behavior of steels on run-out table in hot strip mill, *Journal of materials processing Technology* (2002) **128**:216-225.

[8] Masud A., Tham C.L., Liu W.K.: A stabilized 3-D co-rotational formulation for geometrically nonlinear analysis of multi-layered composite shells, *Comput. Methods. Appl. Mech. Eng.* (2000) **26**:1-12.

[9] Moen C.D., Takeru I., Schafer B.W.: Prediction of residual stresses and strains in cold-formed steel members, *Thin-Walled Structures* (2008) **46**:1274-1289.

[10] Neuschütz E.: *Fließverhalten kaltgewalzter Bänder beim Um- und Aufwickeln*, Directorates-General for Science, Research and Development, Düsseldorf , (1998).

[11] Schwarze M., Vladimirov N., Reese S.: Sheet metal forming and springback simulation by means of a new reduced integration solid-shell finite element technology, *Comput. Methods Appl. Mech. Eng.* (2011) **200**:454-476.

[12] Simo J.C., Miehe J.C.: Associative coupled thermoplasticity at finite strains: formulation numerical analysis and implementation, *Comput. Methods Appl. Mech. Eng.* (1992) **68**:1-31.

[13] Sousa R.J.A., Cardoso R.P.R., Valente R.A.F., Yoon J.W., Gracio J.J., Jorge R.M.N.: A new one-point quadrature enhanced assumed strain (EAS) solid-shell element with multiple integration points along thickness, Part II: Nonlinear applications, *Int. Journal for Num. Meth. Eng.* (2006) **67**:160-188.

[14] Wanga X., Yang Q., He A.: Calculation of thermal stress affecting strip flatness change during run-out table cooling in hot steel strip rolling, *Journal of Materials Processing Technology* (2008) **207**:130-146.

[15] Wilkening H.: *Die Ermittlung der radialen Haspelbelastungen beim Wickeln von bandförmigen Gut*, RWTH-Aachen, Technical report, (1965).

[16] Wriggers P.: *Nichtlineare Finite-Element-Methoden*, Springer, (2000).

[17] Wriggers P.: *Computational Contact Mechanics, Second Edition*, Springer, (2006).

[18] Zhongqing Zhou, Thomson P.F., Yee Cheong Lam, Yuen D.W.: Numerical analysis of residual stress in hot-rolled steel strip on the run-out table, *Journal of Materials Processing Technology* (2003) **132**:184-197.